a common environmental signal in the proxy records because the counts of simultaneous threshold exceedances lie well outside the ranges obtained by the Monte Carlo simulations; (ii) this environmental signal is most likely to be a climate signal because the departures from the Monte Carlo ranges do not just occur during the twentieth century, when very widespread nonclimatic anthropogenic disturbances could arguably have driven a common response in some proxies; (iii) this climate signal is likely to be, at least partly, a temperature indicator, because the proxy records were screened so that only those that were positively correlated with their local instrumental temperatures were selected (table S1); (iv) the analysis of instrumental temperatures indicates that 14 good temperature proxies are sufficient to represent NH mean temperature on 20-year and longer time scales; and (v) the comparison of results using proxy records and instrumental temperatures confirms that the analysis of these proxy records is a useful indicator of NH temperatures.

On this basis it is reasonable to conclude that this study provides evidence for intervals of significant warmth in the NH within the so-called Medieval Warm Period and for significantly colder intervals during the so-called Little Ice Age period. The most widespread and thus strongest evidence indicative of a significantly warm period occurs during the twentieth century [see also Supporting Online Material (SOM) Text], when greenhouse gas concentrations were at their highest during the analysis period. The proxy records indicate that the most widespread warmth occurred in either the mid- or late-twentieth century, but instrumental temperatures provide unequivocal evidence for continuing geographic expansion of anomalous warmth through to the present time.

References and Notes

1. M. E. Mann, R. S. Bradley, M. K. Hughes, *Nature* **392**, 779 (1998).
2. T. J. Crowley, *Science* **289**, 270 (2000).
3. G. C. Hegerl, T. J. Crowley, S. K. Baum, K. Y. Kim, W. T. Hyde, *Geophys. Res. Lett.* **30**, 1242 (2003).
4. P. D. Jones, K. R. Briffa, T. P. Barnett, S. F. B. Tett, *Holocene* **8**, 455 (1998).
5. M. E. Mann, R. S. Bradley, M. K. Hughes, *Geophys. Res. Lett.* **26**, 759 (1999).
6. K. R. Briffa, *Quat. Sci. Rev.* **19**, 87 (2000).
7. T. J. Crowley, T. S. Lowery, *Ambio* **29**, 51 (2000).
8. K. R. Briffa *et al.*, *J. Geophys. Res.* **106**, 2929 (2001).
9. J. Esper, E. R. Cook, F. H. Schweingruber, *Science* **295**, 2250 (2002).
10. T. J. Crowley, S. K. Baum, K. Y. Kim, G. C. Hegerl, W. T. Hyde, *Geophys. Res. Lett.* **30**, 1932 (2003).
11. M. E. Mann, P. D. Jones, *Geophys. Res. Lett.* **30**, 1820 (2003).
12. A. Moberg, D. M. Sonechkin, K. Holmgren, N. M. Datsenko, W. Karlen, *Nature* **433**, 613 (2005).
13. S. Rutherford *et al.*, *J. Clim.* **18**, 2308 (2005).
14. H. N. Pollack, J. E. Smerdon, *J. Geophys. Res.* **109**, D11106 (2004).
15. IPCC, *Climate Change 2001: The Scientific Basis. Contribution of Working Group I to the Third Assessment Report of the Intergovernmental Panel on Climate Change*, J. T. Houghton *et al.*, Eds. (Cambridge Univ. Press, Cambridge, UK, 2001), p. 881.
16. P. D. Jones, T. J. Osborn, K. R. Briffa, *Science* **292**, 662 (2001).
17. P. D. Jones, M. E. Mann, *Rev. Geophys.* **42**, RG2002 (2004).
18. Esper *et al*. (*9*) estimated only the uncertainty of their tree-growth series rather than its representation of NH temperature variability and (*12*) only estimated the uncertainty for time scales of 80 years and longer, which is inappropriate for a formal comparison with the mean temperature of a single decade or even a 30-year period.
19. With inflation to account for autocorrelation in the residuals, and (*16*) included additional uncertainty associated with the regression model coefficients.
20. P. D. Jones, K. R. Briffa, T. J. Osborn, *J. Geophys. Res.* **108**, 4588 (2003).
21. G. R. Bigg, T. D. Jickells, P. S. Liss, T. J. Osborn, *Int. J. Climatol.* **23**, 1127 (2003).
22. H. von Storch *et al.*, *Science* **306**, 679 (2004); published online 30 September 2004 (10.1126/science.1096109).
23. We note first that the bias may be smaller than indicated by (*22*) [see (*32*, *33*)] and second that this bias affects the coldest periods much more than temperatures that are of comparable warmth to the calibration period.
24. W. Soon, S. Baliunas, *Clim. Res.* **23**, 89 (2003).
25. M. Mann *et al.*, *Eos* **84**, 256 (2003).
26. Materials and methods are available as supporting material at *Science* Online.
27. The percentiles of the Monte Carlo distributions are nearer to zero then, and thus smaller anomalies may still be significant.
28. P. D. Jones, A. Moberg, *J. Clim.* **16**, 206 (2003).
29. H. H. Lamb, *Climate History and the Future, Vol. 2, Climate: Present, Past and Future* (Methuen, New York, 1977), p. 835.
30. A. E. J. Ogilvie, T. Jonsson, *Clim. Change* **48**, 9 (2001).
31. J. Esper, D. C. Frank, R. J. S. Wilson, K. R. Briffa, *Geophys. Res. Lett.* **32**, L07711 (2005).
32. T. J. Osborn, S. C. B. Raper, K. R. Briffa, *Clim. Dyn.*, in press.
33. M. E. Mann, S. Rutherford, E. Wahl, C. Ammann, *J. Clim.* **18**, 4097 (2005).

34. Supported by the European Community under research contract EVK2-CT2002-00160 SOAP. M. Mann, P. Jones, J. Esper, and E. Cook are thanked for making proxy data records available to us.

Supporting Online Material

www.sciencemag.org/cgi/content/full/311/5762/841/DC1
Materials and Methods
SOM Text
Figs. S1 to S6
Tables S1 and S2

23 September 2005; accepted 17 January 2006
10.1126/science.1120514

Histone H4-K16 Acetylation Controls Chromatin Structure and Protein Interactions

Michael Shogren-Knaak,[1]*† Haruhiko Ishii,[1]* Jian-Min Sun,[2] Michael J. Pazin,[3] James R. Davie,[2] Craig L. Peterson[1]‡

Acetylation of histone H4 on lysine 16 (H4-K16Ac) is a prevalent and reversible posttranslational chromatin modification in eukaryotes. To characterize the structural and functional role of this mark, we used a native chemical ligation strategy to generate histone H4 that was homogeneously acetylated at K16. The incorporation of this modified histone into nucleosomal arrays inhibits the formation of compact 30-nanometer–like fibers and impedes the ability of chromatin to form cross-fiber interactions. H4-K16Ac also inhibits the ability of the adenosine triphosphate–utilizing chromatin assembly and remodeling enzyme ACF to mobilize a mononucleosome, indicating that this single histone modification modulates both higher order chromatin structure and functional interactions between a nonhistone protein and the chromatin fiber.

DNA in eukaryotes is present as chromatin, which is an assembly of histones, DNA, and chromatin-associated proteins. The basic building block of chromatin is the nucleosome, which contains two copies of histones H2A, H2B, H3, and H4 (*1*). Fifteen to 38 amino acids from each histone N terminus form the histone "tails," providing a platform for posttranslational modifications that modulate the biological role played by the underlying DNA (*2*). One prevalent modification is H4-K16Ac (*3*), which has roles in transcriptional activation and the maintenance of euchromatin (*4*, *5*).

Recent work has focused on the ability of histone marks to modulate the binding of nonhistone proteins to the chromatin fiber, such as the yeast silencing factor Sir3 and the *Drosophila* chromatin-remodeling enzyme ISWI (*6*, *7*). We were interested in testing whether histone modifications might control higher order chromatin structures. Indeed, random hyperacetylation of histone tails (>6 acetates per octamer) disrupts intramolecular folding of nucleosomal arrays into compact, 30-nm-thick fibers (*8*). Additionally, the H4 tail, and particularly residues 14 to 23, are uniquely important for the formation of these fibers (*1*, *9*). The acetylation of H4-K16 occurs within this region, providing a potential mechanism to regulate chromatin folding.

We used a native chemical ligation strategy to generate recombinant histone H4 homogeneously acetylated at K16 (*10*, *11*). In this strategy, an H4 N-terminal peptide (amino acids 1 to 22), with a C-terminal thioester and an acetylated lysine 16, was synthesized. A recombinant

C-terminal fragment of histone H4 (amino acids 23 to 102), in which H4 arginine 23 (R23) had been changed to a cysteine (R23C), was expressed and purified (fig. S1). Chemical ligation of these components yielded full-length H4-K16Ac (Fig. 1A). This product is the same length as unacetylated histone H4 (Fig. 1B) but demonstrates an expected reduction in charge (fig. S2). Three additional H4 polypeptides were expressed and purified (fig. S1): (i) wild-type (WT) H4; (ii) H4-R23C, which harbors the same cysteine substitution present in ligated H4; and (iii) H4-ΔN, in which the N-terminal tail (residues 1 to 19) has been deleted. All H4 polypeptides were incorporated into histone octamers containing recombinant H2A, H2B, and H3 (*1*), and neither H4-K16Ac nor ligation interfered with octamer assembly (Fig. 1B).

Using step-wise salt dialysis, the four distinct histone octamers were assembled into nucleosomal arrays with a DNA template that harbors 12 copies of the 177–base pair "601" nucleosome positioning sequence (601-177-12) (*9*, *12*). In order to ensure that each DNA template was saturated with 12 nucleosomes, octamers were added in slight excess to the number of 601 repeats, and mononucleosomal-length DNA was included in the reconstitution reactions to act as an "octamer sink" (Fig. 1C) (*9*). After assembly, 601-177-12 nucleosomal arrays were purified from mononucleosomes by selective $MgCl_2$ precipitation (Fig. 1C), and array saturation was confirmed (fig. S2).

We used sedimentation velocity in conjunction with van Holde–Weischet analysis (*13*) to ascertain the distribution of sedimentation coefficients for the population of nucleosomal arrays within a sample. Saturated arrays containing H4-WT (Fig. 2A, diamonds), H4-R23C (circles), H4-K16Ac (squares), and H4-ΔN octamers (triangles) were sedimented in a buffer lacking divalent cations, conditions in which nucleosomal arrays adopt an extended "beads-on-a-string" conformation. Each of the four arrays showed nearly identical distributions of sedimentation coefficients (S), with expected midpoints between 34 and 36 S (Fig. 2A, open symbols) (*9*, *14*).

When wild-type (Fig. 2E, solid diamonds) and H4-R23C (solid circles) arrays were incubated in a buffer containing 1.0 mM $MgCl_2$, they formed more compact fibers that shifted the sedimentation coefficient distributions to midpoints between 53 and 54 S. These results are consistent with the formation of compact, 30-nm–like fibers, and the H4-R23C substitution does not disrupt this condensation reaction. In contrast, and consistent with a previous report (*9*), the array reconstituted with H4 that lacks an N-terminal tail (H4-ΔN) (Fig. 2C, solid squares) was unable to condense fully, reaching a midpoint of only 44S. The array reconstituted with H4-K16Ac displayed an identical defect in $MgCl_2$-dependent compaction (Fig. 2A, solid triangles), suggesting that the acetylation of a single lysine leads to a chromatin folding defect equivalent to deletion of the entire H4 tail.

We also analyzed a large set (>10) of different subsaturated arrays (<12 nucleosomes

[1]Program in Molecular Medicine, University of Massachusetts Medical School, Worcester, MA 01605, USA. [2]Manitoba Institute of Cell Biology, University of Manitoba, Winnipeg, Manitoba R3E0V9, Canada. [3]Laboratory of Cellular and Molecular Biology, National Institute on Aging, National Institutes of Health, 5600 Nathan Shock Drive, Baltimore, MD 21224, USA.

*These authors contributed equally to this work.
†Present address: Department of Biochemistry, Biophysics, and Molecular Biology, Iowa State University, 4214 Molecular Biology Building, Ames, IA 50011, USA.
‡To whom correspondence should be addressed. E-mail: craig.peterson@umassmed.edu

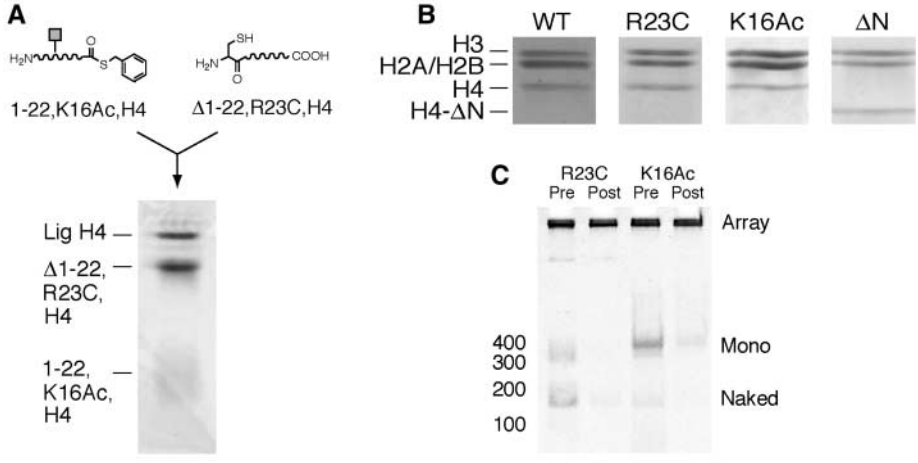

Fig. 1. Histone H4-K16Ac is incorporated into nucleosomal arrays. (**A**) Ligation of K16Ac-containing peptide and H4 C-terminal fragment. A ligation reaction is separated on 18% SDS-PAGE gel and stained with Coomassie (*27*). (**B**) Shown are peak fractions of H4-WT–, H4-R23C– H4-K16Ac–, or H4-ΔN–containing histone octamers isolated by gel filtration, separated on 18% SDS-PAGE gel, and stained with Coomassie. (**C**) Nucleosomal arrays containing histone H4-K16Ac prepared in the presence of 174–base pair (bp) 5S DNA. Nucleosomal arrays before (pre) and after (post) precipitation with 4.0 mM $MgCl_2$ analyzed on native 4% PAGE and stained with ethidium bromide are shown. Shown is a typical gel obtained with saturated arrays containing histone H4-R23C or histone H4-K16Ac. Mono and Naked indicate 5S mononucleosomes and free DNA, respectively.

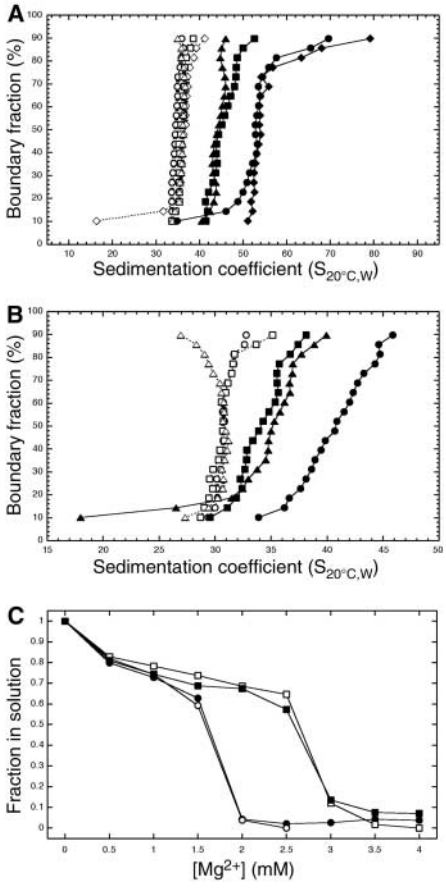

Fig. 2. H4-K16Ac abolishes higher order chromatin structure. (**A**) H4-K16Ac abolishes folding of nucleosomal arrays. Integrated sedimentation coefficient distributions of nucleosomal arrays in the presence and absence of Mg^{2+} were determined by using sedimentation velocity and van Holde-Weischet analysis. Arrays containing WT, H4-R23C, H4-K16Ac, and H4-ΔN histones are depicted by diamonds, circles, squares, and triangles, respectively. Arrays analyzed in the absence (0.1mM ethylenediaminetetraacetic acid) or presence of Mg^{2+} (1.0 mM $MgCl_2$) are shown as open or solid symbols, respectively. $S_{20°C,W}$ is the sedimentation coefficient corrected to water at 20°C and adjusted for the difference in mass of the H4-ΔN histone. The data shown are representative of 3 to 5 array reconstitutions. (**B**) Subsaturated arrays containing H4-K16Ac. Analysis was performed as in (**A**). Data shown are representative of at least 3 to 5 array reconstitutions. (**C**) H4-K16Ac disrupts array oligomerization. Nucleosomal arrays were incubated with varying concentrations of $MgCl_2$ at room temperature for 15 min, followed by centrifugation in a microfuge. The fraction of array remaining in the supernatant is plotted as a function of $MgCl_2$ concentration. Arrays containing WT, H4-R23C, H4-K16Ac, and H4-ΔN histones are depicted by solid circles, open circles, open squares, and solid squares, respectively.

per template) reconstituted with the four different octamers (Fig. 2B) (*15*). In every case, the addition of $MgCl_2$ to the wild-type and H4-R23C arrays led to large increases in the sedimentation coefficient distributions, consistent with salt-dependent compaction. However, arrays reconstituted with the H4-ΔN and H4-K16Ac octamers were again equally defective for $MgCl_2$-dependent compaction at every level of saturation (Fig. 2B) (*15*).

As the concentration of $MgCl_2$ was increased beyond 1.5 mM, arrays underwent reversible self-association that is believed to mimic fiber-fiber interactions that stabilize higher order chromosomal domains (*16*). For the 601-177-12 arrays, the deletion of the H4 tail disrupted self-association (*9*). To test whether H4-K16Ac affects this intermolecular interaction, arrays reconstituted with H4-WT, H4-R23C, H4-K16Ac, and H4-ΔN octamers were assayed. Self-association of the H4-WT and H4-R23C arrays (Fig. 2C, solid and open circles, respectively) occurred at magnesium concentrations of 1.5 to 2.0 mM, comparable to previously reported values (*9*). In contrast, self-association of the H4-ΔN and H4-K16Ac arrays (Fig. 2C, solid and open squares, respectively) both required higher concentrations of $MgCl_2$ (2.5 to 3.0 mM). Thus, as in the case for intramolecular folding, the single acetylation of H4-K16 cripples the self-association of arrays and shows defects equivalent to the loss of the H4 tail.

Next we investigated whether H4-K16Ac is associated with decondensed chromatin structures in vivo. HeLa nuclei were digested with micrococcal nuclease (Mnase), and the released chromatin fractionated into $MgCl_2$-soluble and $MgCl_2$-insoluble components. Samples were separated on an SDS–polyacrylamide gel and on an acid-urea-triton (AUT) gel, and the abundance of H4-K16Ac was analyzed by Western blotting (Fig. 3). Consistent with the biochemical studies, H4-K16Ac was enriched in the $MgCl_2$-soluble chromatin fractions (Fig. 3, A and B) that are also enriched in transcriptionally active gene sequences (*17*). Furthermore, the $MgCl_2$-soluble fractions contained an H4 tail that is exclusively monoacetylated at H4-K16 (Fig. 3B).

We also tested whether nucleosomal H4-K16Ac affects interactions with chromatin-associated proteins, specifically the *Drosophila* ISWI-containing adenosine triphosphate (ATP)–utilizing chromatin assembly and remodeling enzyme (ACF) complex. This complex hydrolyzes ATP to mediate nucleosome sliding in cis along DNA (*18*). This activity requires residues 16 to 19 of the H4 tail (*19*, *20*), and in vitro peptide competition assays have suggested that H4-K16Ac may reduce the interaction of ISWI with nucleosomes (*7*). To test directly the effect of H4-K16Ac on ISWI activity, we reconstituted end-positioned mononucleosomes with wild-type, H4-R23C, and H4-K16Ac octamers. Each of these mononucleosomes was incubated with the ACF complex, and ATP-dependent mobilization of nucleosomes was analyzed by native polyacrylamide gel electrophoresis (PAGE). When wild-type nucleosomes were incubated with ACF and ATP, a slower-migrating species accumulated with time (half-time $t_{1/2}$ = ~7.5 min) (Fig. 4.). This shift in electrophoretic mobility depended on the presence of both ACF and ATP, and it likely represents sliding of the nucleosome to a more central position. This ACF activity was also detected on mononucleosomes reconstituted with H4-K16Ac, but in this case, sliding was slower as compared to the WT and H4-R23C substrates ($t_{1/2}$ = ~20 min). These results are consistent with previous peptide studies, demonstrating that H4-K16Ac regulates the functioning of a chromatin-remodeling enzyme independent of its effects on chromatin higher order structure.

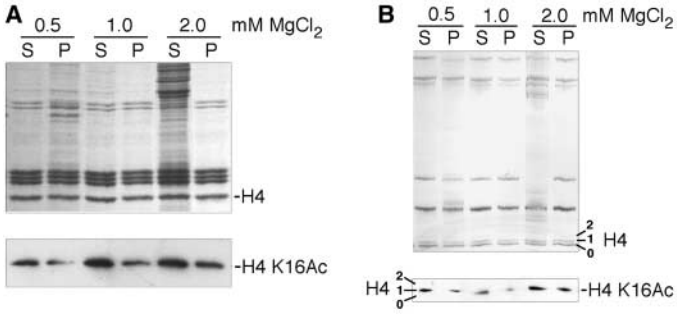

Fig. 3. H4-K16Ac is enriched in $MgCl_2$-soluble chromatin. HeLa nuclei were digested with micrococcal nuclease, and the solubilized chromatin was incubated with $MgCl_2$ at different final concentrations of 0.5, 1, or 2 mM for 10 min on ice. Histones from the magnesium soluble (S) and insoluble (P) chromatin fractions were electrophoresed on (**A**) 15% SDS-PAGE gels or (**B**) 15% AUT-PAGE gels. The AUT gel separates the acetylated histone isoforms. The top panels display Coomassie blue–stained gels and the bottom panels show Western analyses with antibodies to H4-K16Ac (Upstate, Charlottesville, VA).

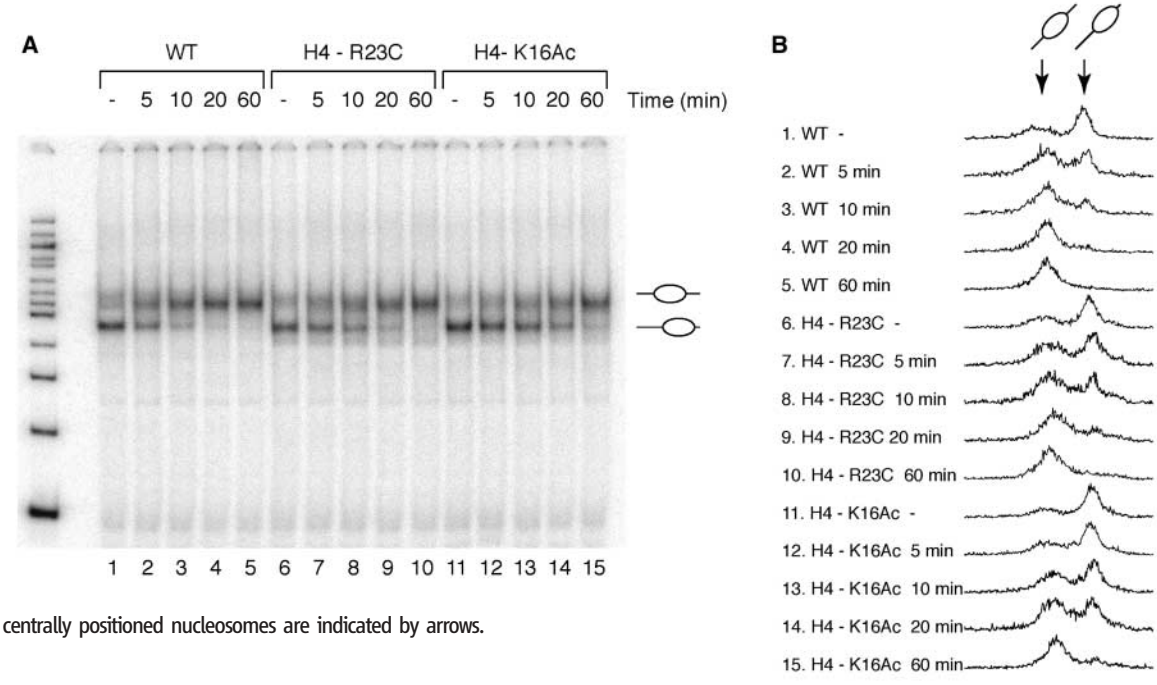

Fig. 4. H4-K16Ac inhibits ACF-mediated nucleosome sliding. (**A**) End-positioned nucleosomes containing indicated histone H4 were incubated with ACF and ATP at 30°C. Samples were taken from reactions at indicated times and quenched by the addition of EDTA and by placing them on ice. Samples were separated by electrophoresis on 4% native polyacrylamide gels. Lanes 1, 6, and 11 show mononucleosomes without incubation with ACF. (**B**) Profiles of gel lanes shown in (A). Peaks corresponding to the predicted end-positioned and centrally positioned nucleosomes are indicated by arrows.

The structural effect of H4-K16Ac may directly contribute to regions of decondensed chromatin in eukaryotic organisms. In budding yeast, over 80% of H4 is acetylated at lysine 16, and most of the genome exists in a decondensed state (*3*, *21*). Likewise, evidence suggests that the transcriptionally enhanced X chromosome of male flies, a site of ubiquitous H4-K16Ac, is decondensed (*22*). Such decondensation of chromatin may contribute to the establishment of transcriptionally active euchromatic regions. In vitro transcription studies suggest that the adoption of higher order chromatin structure reduces gene transcription (*23*). In contrast, acetylation of H4-K16 increases gene transcription both in vitro and in vivo (*24*), and the decompaction resulting from such modification may increase the accessibility of factors that promote transcription.

Do other histone marks regulate chromatin folding? The phosphorylation of H3-S10 (S, serine) does not disrupt chromatin folding (*25*), and triacetylation of the H3 tail by Gcn5p does not disrupt chromatin compaction (*26*). Similarly, residues 1 to 13 of histone H4 that include three sites of acetylation are dispensable for folding of 601-177-12 arrays (*9*). Thus, H4-K16 is likely to be a unique acetylation site of histone tails, which function as a dual switch for higher order chromatin structure and protein-histone interactions, promoting chromatin function in a mutually reinforcing manner.

References and Notes

1. K. Luger, A. W. Mader, R. K. Richmond, D. F. Sargent, T. J. Richmond, *Nature* **389**, 251 (1997).
2. C. L. Peterson, M. A. Laniel, *Curr. Biol.* **14**, R546 (2004).
3. C. M. Smith *et al.*, *Anal. Biochem.* **316**, 23 (2003).
4. A. Hilfiker, D. Hilfiker-Kleiner, A. Pannuti, J. C. Lucchesi, *EMBO J.* **16**, 2054 (1997).
5. N. Suka, K. Luo, M. Grunstein, *Nat. Genet.* **32**, 378 (2002).
6. A. Hecht, T. Laroche, S. Strahl-Bolsinger, S. M. Gasser, M. Grunstein, *Cell* **80**, 583 (1995).
7. D. F. Corona, C. R. Clapier, P. B. Becker, J. W. Tamkun, *EMBO Rep.* **3**, 242 (2002).
8. C. Tse, T. Sera, A. P. Wolffe, J. C. Hansen, *Mol. Cell. Biol.* **18**, 4629 (1998).
9. B. Dorigo, T. Schalch, K. Bystricky, T. J. Richmond, *J. Mol. Biol.* **327**, 85 (2003).
10. P. E. Dawson, T. W. Muir, I. Clark-Lewis, S. B. Kent, *Science* **266**, 776 (1994).
11. M. A. Shogren-Knaak, C. L. Peterson, *Methods Enzymol.* **375**, 62 (2004).
12. P. T. Lowary, J. Widom, *J. Mol. Biol.* **276**, 19 (1998).
13. K. E. van Holde, W. O. Weischet, *Biopolymers* **17**, 1387 (1978).
14. B. Dorigo *et al.*, *Science* **306**, 1571 (2004).
15. M. A. Shogren-Knaak, H. Ishii, C. L. Peterson, data not shown.
16. P. M. Schwarz, A. Felthauser, T. M. Fletcher, J. C. Hansen, *Biochemistry* **35**, 4009 (1996).
17. J. R. Davie, E. P. Candido, *Proc. Natl. Acad. Sci. U.S.A.* **75**, 3574 (1978).
18. A. Eberharter, G. Langst, P. B. Becker, *Methods Enzymol.* **377**, 344 (2004).
19. A. Hamiche, J. G. Kang, C. Dennis, H. Xiao, C. Wu, *Proc. Natl. Acad. Sci. U.S.A.* **98**, 14316 (2001).
20. C. R. Clapier, G. Langst, D. F. Corona, P. B. Becker, K. P. Nightingale, *Mol. Cell. Biol.* **21**, 875 (2001).
21. D. Lohr, R. T. Kovacic, K. E. Van Holde, *Biochemistry* **16**, 463 (1977).
22. C. A. Offermann, *J. Genet.* **32**, 103 (1936).
23. J. C. Hansen, A. P. Wolffe, *Biochemistry* **31**, 7977 (1992).
24. A. Akhtar, P. B. Becker, *Mol. Cell* **5**, 367 (2000).
25. C. J. Fry, M. A. Shogren-Knaak, C. L. Peterson, *Cold Spring Harb. Symp. Quant. Biol.* **69**, 219 (2004).
26. J. C. Hansen, personal communication.
27. Materials and methods are available as supporting material on *Science* Online.

28. This work was supported by a grant from NIH to C.L.P. (GM54096). M.J.P. was supported by the Intramural Research Program of NIH, National Institute on Aging. J.R.D. was supported by a grant from the Canadian Institute of Health Research (MOP-9186). We thank T. Richmond for providing the 601-177-12 array template.

Supporting Online Material

www.sciencemag.org/cgi/content/full/311/5762/844/DC1
Materials and Methods
Figs. S1 to S3
References

19 December 2005; accepted 9 January 2006
10.1126/science.1124000

Caspases 3 and 7: Key Mediators of Mitochondrial Events of Apoptosis

Saquib A. Lakhani,[1,2] Ali Masud,[1,2] Keisuke Kuida,[6] George A. Porter Jr.,[2] Carmen J. Booth,[3] Wajahat Z. Mehal,[1,4] Irteza Inayat,[4] Richard A. Flavell[1,5]*

The current model of apoptosis holds that upstream signals lead to activation of downstream effector caspases. We generated mice deficient in the two effectors, caspase 3 and caspase 7, which died immediately after birth with defects in cardiac development. Fibroblasts lacking both enzymes were highly resistant to both mitochondrial and death receptor–mediated apoptosis, displayed preservation of mitochondrial membrane potential, and had defective nuclear translocation of apoptosis-inducing factor (AIF). Furthermore, the early apoptotic events of Bax translocation and cytochrome c release were also delayed. We conclude that caspases 3 and 7 are critical mediators of mitochondrial events of apoptosis.

Mitochondria play a central role in apoptosis. Mitochondrial outer membrane permeabilization (MOMP) leads to release of proapoptotic factors such as cytochrome c and AIF (*1*). Furthermore, loss of mitochondrial membrane potential ($\Delta\psi_m$) is thought to contribute to cell death by disruption of normal mitochondrial function (*2*, *3*). Interaction of members of the Bcl-2 family of proteins regulates MOMP, the key event of cytochrome c release into the cytoplasm (*3*, *4*). What is less clear, however, is the precise role of caspase proteases in mitochondrial events of apoptosis. Although upstream caspases, such as caspase 2 and caspase 8, affect mitochondrial events in both death-receptor and mitochondrial pathways of apoptosis, either directly or through interaction with Bcl-2 family members, the role of presumed downstream "effector" caspases in this process is less clear (*5*, *6*). Therefore, we studied the two highly related effectors, caspase 3 and caspase 7, to elucidate their functions in apoptosis.

We generated caspase $7^{-/-}$ mice (fig. S1), which were born in ratios consistent with Mendelian inheritance. They had normal appearance, organ morphology, and lymphoid development. When caspase $7^{-/-}$ mouse embryonic fibroblasts (MEFs) were treated with inducers of apoptosis, they exhibited a slight survival advantage as compared with wild-type MEFs. Apoptosis caused by a range of insults in other caspase $7^{-/-}$ cells proceeded normally, however, including the death of activated T cells following stimulation of the T cell receptor, thymocyte apoptosis, Fas-mediated death of B cells, and Fas-mediated death of hepatocytes (fig. S2).

Caspase 3, which is structurally similar to caspase 7, might compensate for the lack of caspase 7, which would lead to this relatively mild antiapoptotic phenotype (*7*, *8*). Thus, we bred caspase $7^{-/-}$ mice to caspase $3^{-/-}$ mice previously described by our laboratory (*9*). The embryonic stem cells containing the mutation were from the 129/SvJ genetic background. Mice derived from these embryonic stem cells were backcrossed six generations onto the C57BL/6 background. We obtained no live caspase $3^{-/-}$/caspase $7^{-/-}$ double-knockout (DKO) mice when progeny were genotyped at an age of 10 to 14 days. DKO mice were present at normal Mendelian numbers through embryonic day 20 (E20), but died rapidly after birth. A small percentage (~10%) of both caspase $3^{-/-}$/caspase $7^{+/-}$ and DKO embryos displayed exencephaly, likely due to the absence of caspase 3 in combination with residual genes from the 129/SvJ background (*10*). The major-

[1]Section of Immunobiology; [2]Department of Pediatrics; [3]Section of Comparative Medicine; [4]Department of Internal Medicine, [5]Howard Hughes Medical Institute, Yale University School of Medicine, New Haven, CT 06520, USA. [6]Vertex Pharmaceuticals, 130 Waverly Street, Cambridge, MA 02139, USA.

*To whom correspondence should be addressed. E-mail: richard.flavell@yale.edu

Supporting Online Material for

Histone H4-K16 Acetylation Controls Chromatin Structure and Protein Interactions

Michael Shogren-Knaak, Haruhiko Ishii, Jian-Min Sun, Michael J. Pazin, James R. Davie, Craig L. Peterson*

*To whom correspondence should be addressed. E-mail: craig.peterson@umassmed.edu

Published 10 February 2006, *Science* **311**, 844 (2006)
DOI: 10.1126/science.1124000

This PDF file includes:

Supporting Online Material

Materials and methods

Generation of H4-R23C, H4-ΔN, and Wildtype Histones

To construct the bacterial expression vector for histone H4 R23C, QuikChange mutagenesis (Stratagene) was performed on the Xenopus laevis H4 expression vector (*1*) using the following primers: 5'-CAC CGT AAA GTT CTG TGT GAC AAC ATC CAG GG-3' and 5'-CCC TGG ATG TTG TCA CAC AGA ACT TTA CGG TG-3'. Presence of the desired mutation was confirmed by DNA sequencing of the full histone sequence. Expression and purification of the mutated H4 histone, as well as the H4-ΔN and wildtype histones (H2A, H2B, H3, and H4) (*1*), was performed according to standard protocols (*2*). In brief, histone is induced in BL21(DE3) pLysS cells, isolated as inclusion bodies, purified by Sephacryl S-200 gel filtration and SP-HR ion exchange chromatography, dialyzed against a 1.0 mM DTT solution, and lyophilized, to give pure recombinant histone.

Generation of H4 K16Ac Histone

To construct a bacterial expression vector for histone H4 Δ1-22 R23C mutation, Xenopus laevis histone H4 (*1*) coding sequence was amplified with PCR using the primers 5'-ACC GTA AAC ATA TGT GTG ACA ACA TCC AGG GTA TCA C-3' and 5'-CAG CCG GAG ATC TTA ACC ACC GAA ACC GTA CAG-3'. The PCR product was digested with Nde I and Bgl II and was cloned into pET3c digested with Nde I and BamHI. Expression and purification of the truncated histone was performed as described above for the other histones, with the exceptions that induction was performed in BL21(DE3) cells, and that following ion exchange purification, the histone was dialyzed once against a 5mM DTT solution, and at least two times against a 0.05% trifluoroacetic acid solution.

H4 peptide containing residues 1-22 was synthesized using standard Fmoc-based solid-phase peptide synthesis. Amino acid 22, leucine, was preloaded on the 2-Chlorotrityl residue (NovaBiochem). Acetyllysine was incorporated directly during synthesis using commercially available Fmoc-Lys(Ac)-OH (NovaBiochem). Installation of the C-terminal thioester was performed as described previously, where the peptide is cleaved from the resin with side-chain protecting groups, thioesterified at the C-terminus, and then side-chain deprotected (*3*). Thioester peptide was isolated by C_{18} reversed-phase HPLC purification. Quantification of the peptide was estimated by weight. The identity and purity of the thioester peptide was confirmed by MALDI-TOF mass spectrometry.

Ligation of the H4 Δ1-22 R23C and H4 1-22 K16Ac thioester fragments was performed as described for ligation of H3 histones (*3*), where ligation under denaturing conditions is followed by isolation of the desired product by ion exchange chromatography. The sole difference was that following the chromatographic purification, the ligated H4 product was not lyophilized, but instead was used directly in the octamer reconstitution step. Identity and purity of the ligated product was confirmed by SDS-PAGE and AUT gel analysis, as well as by MALDI-TOF mass spectrometry.

Nucleosomal Array Reconstitutions

Histone octamers were prepared by denaturing the histones followed by dialysis into 2.0 M NaCl according to standard protocols (*2*), with the exception that ligated H4 K16Ac histone was utilized directly following ion exchange purification. Quantification of the histones was performed at 276 nm and 320 nm as described (*2*). 601-177-12 template DNA was excised from plasmid containing this sequence using ScaI (*4*) and purified by gel filtration chromatography as performed for other nucleosomal templates (*5*). 174 bp 5S rDNA sequence was generated by PCR amplification of EcoRI digested 208-12 5S rDNA (*5*) with the primers 5'- CTC CCA TCC AAG TAC TAA CCG AGC CC –3' and 5'- CCA ACG AAT AAC TTC CAG GGA TTT ATA AGC CG –3'. PCR product was purified by preparative gel electrophoresis and electroelution.

Nucleosomal arrays were assembled with 601-177-12 DNA template and histone octamers largely as described by Richmond and coworkers (*4*). In a typical reconstitution, 1.15 equivalent of histone octamer (42.5 μg), 1.0 equivalents of 601-177-12 template (23.7 μg), 0.3 equivalents of 174 bp 5S rDNA (14.5 μg), and 5.0 M NaCl were combined to generate a solution with a final concentration of 2.0 M NaCl (500 μl final volume). Octamer is deposited onto the DNA template by step dialysis into decreasing concentration of salt: 1.4 M NaCl, 1.2 M NaCl, 0.8 M NaCl, 0.6 M NaCl (all with 10 mM Tris pH 8.0, 0.25 mM EDTA, and 1.0 mM DTT), followed by exchanges with 2.5 mM NaCl, 10 mM HEPES, and 0.1% TCEP. Removal of mononucleosome and free 174 bp 5S rDNA was accomplished by precipitation with an equal volume of 8.0 mM $MgCl_2$ (*4*). The extent of 601-177-12 purification is monitored by resolving the DNA products on a 4% native polyacrylamide gel (4% acrylamide, 0.11% bis-acrylamide, 1.0x TBE) in 1.0 x TBE, and staining of the DNA by ethidium bromide. The extent of saturation of the purified arrays is ascertained by ScaI digestion (400 ng total DNA, 2 units ScaI, 50 mM NaCl, 50 mM Tris pH 7.4, 0.5 mM $MgCl_2$, 12 hours at room temperature), followed by analysis using a 4% native polyacrylamide gel as above. Varying array saturation is accomplished by varying the initial histone octamer amounts.

Nucleosomal Array Folding Assays

Nucleosomal arrays with an A_{260} between 0.6 and 1.6 were diluted 1:1 in a solution of either 2x EDTA (2.5 mM NaCl, 10 mM HEPES pH 8.0, 0.1 mM TCEP, 0.2 mM EDTA) or 2x folding buffer (2.5 mM NaCl, 10mM HEPES pH 8.0, 0.1 mM TCEP, and 2.0 mM $MgCl_2$) and allowed to equilibrate to room temperature. Samples were loaded into cells, placed in an An60 Ti rotor in a Beckman Optima XL-I analytical ultracentrifuge, and equilibrated at 20 °C under vacuum for at least two hours. Time-dependent sedimentations of the arrays was monitored at 260 nm at a speed of at least 12,000 RPM. Boundaries were analyzed by the method of van Holde and Weichet (*6*) using Ultrascan 5.0. Data were plotted as boundary fraction (y-axis) versus $S_{20,w}$ (sedimentation corrected to water at 20 °C) to yield the integrated sedimentation velocity distribution. The

sedimentation distribution for arrays containing H4 ΔN was normalized for mass relative to the other arrays.

Nucleosomal Array Self-association Assays

Nucleosomal arrays were diluted to A_{260} ~ 0.4. Equal volumes of nucleosomal arrays and 2x $MgCl_2$ solutions were mixed. Samples were incubated at room temperature for >15 min, followed by centrifugation at 14,000 g for 10 min. The supernatant of each sample was collected and the absorbance at 260 nm was measured. Fraction in solution was calculated by normalizing A_{260} at each magnesium concentration to that of 0 mM magnesium.

Reconstitution of Mononucleosomes and ACF-dependent Sliding

End-positioned mononucleosomes were reconstituted with a DNA fragment containing 601 nucleosome positioning sequence close to one end. A 246-bp DNA fragment was generated by PCR amplification of plasmid CP1024 with the primers 5'-GGG CGA ATT CGA GCT CGG TAC C-3' and 5'-GAA GAT CTC GCC CTG GAG AAT CCC-3'. The PCR product was digested with BglII and was radioactively labeled by filling in the restriction site with dATP, [α-^{32}P] dCTP, dGTP, and dTTP using Klenow enzyme. The radioactive DNA fragment was mixed with excess of cold DNA fragment. Mononucleosomes were reconstituted by mixing the DNA fragment with histone octamers with total DNA to octamer ratio of approximately 1:1 (mol/mol), followed by step-wise salt dialysis.

55 nM mononucleosome was incubated with 1.5 nM recombinant ACF and 0.2 mM ATP in a reaction buffer (20 mM Tris-HCl [pH8.0], 75 mM NaCl, 5 mM $MgCl_2$, 0.2 mM dithiothreitol, 0.1% Tween-20, 0.1 mg/ml bovine serum albumin, 5% glycerol) at 30 ˚C. 12 μl samples were taken at indicated times, mixed with 3 μl stop solution (0.1 M EDTA, 40% glycerol) and incubated on ice until electrophoresis. Samples were resolved by electrophoresis on 4% 1x Tris-borate-EDTA (TBE) native acrylamide gels and imaged using a Molecular Dynamics PhosphorImager.

Determination of H4 K16Ac enrichment in $MgCl_2$-soluble chromatin

Chromatin fractionation of HeLa cells was prepared as described previously (*7*) with some modifications. HeLa nuclei were digested with micrococcal nuclease and the soluble chromatin (SE) was extracted in the presence of 0.1mM EDTA. Approximately 30 A_{260} of chromatin was incubated with $MgCl_2$ at different final concentrations of 0.5, 1 or 2 mM for 10 min on ice. The magnesium soluble (S) and insoluble (P) chromatin fractions were collected by centrifugation. Total histones were extracted from chromatin fractions with 0.4N sulfuric acid. Ten μg of histone were electrophoresed onto SDS 15% PAGE gels or AUT 15% PAGE gels. Protein was detected either by Coomassie blue-staining or by immunochemical staining of nitrocellulose membranes with anti-H4-K16ac antibodies (Upstate). The amount of magnesium insoluble chromatin (Mg-insoluble % = 1- [A_{260} (Mg-soluble) / A_{260} (input)]) for each magnesium concentration was determined to be: 0.5 mM: 31.7 (+/- 0.9) %; 1.0 mM: 81.1 (+/- 3.2) %; 2.0 mM:

96.9 (+/- 0.2) %.

1. K. Luger, T. J. Rechsteiner, T. J. Richmond, *Methods Mol. Biol.* **119**, 1-16 (1999).
2. K. Luger, T. J. Rechsteiner, T. J. Richmond, *Methods Enzymol.* **304**, 3-19 (1999).
3. M. A. Shogren-Knaak, C. L. Peterson, *Methods Enzymol.* **375**, 62-76 (2004).
4. B. Dorigo, T. Schalch, K. Bystricky, T. J. Richmond, *J. Mol. Biol.* **327**, 85-96 (Mar 14, 2003).
5. L. M. Carruthers, C. Tse, K. P. Walker, 3rd, J. C. Hansen, *Methods Enzymol.* **304**, 19-35 (1999).
6. K. E. van Holde, W. O. Weischet, *Biopolymers* **17**, 1387-1403 (1978).
7. G. P. Delcuve, J. R. Davie, *Biochem. J.* **263**, 179-86 (Oct 1, 1989).

Figures and legends

Fig S1. Amino-terminal sequences of the H4 histones studied. Lysine 16 is shown in bold with a square depicting the acetyl group. Ligation occurs at the site denoted by the triangle and requires cysteine at position 23, also indicated in bold.

Fig S2. Ligated histone H4-K16Ac is homogeneously acetylated at a single site. Histone octamers were separated by charge on a Acetic Acid-Urea-Triton gel and stained with Coomassie blue. For comparison, H4-WT octamer (no loss of charge), H4-R23C octamer (loss of a single charge), and H4-K16Ac octamer (loss of two charges) are shown. Data shown are representative of several, independent ligation reactions and histone octamer assemblies.

Fig S3. Arrays prepared from histone H4-K16Ac form saturated nucleosomal arrays. Purified nucleosomal arrays were cleaved with ScaI, a restriction enzyme that cleaves between every nucleosome positioning site. Digestion products were electrophoresed on a native 4% PAGE gel, and stained with ethidium bromide. Shown is a typical gel obtained with saturated array containing either histone H4-R23C or histone H4-K16Ac. 'Mono' and 'Naked' indicate 601-177 mononucleosomes and free DNA, respectively Observed are almost exclusively mononucleosome products.

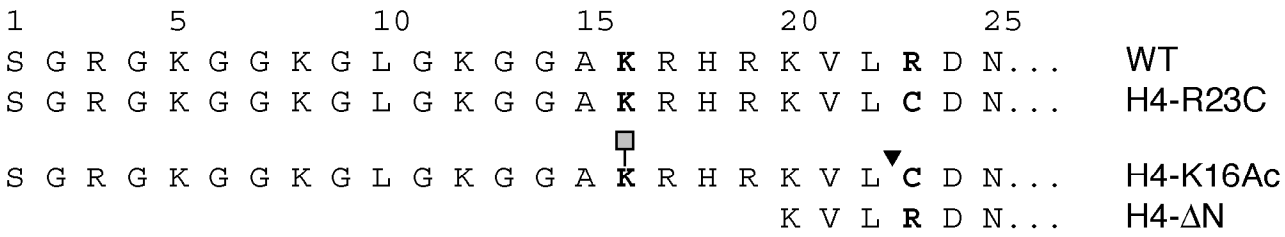

Supplemental Figure 1

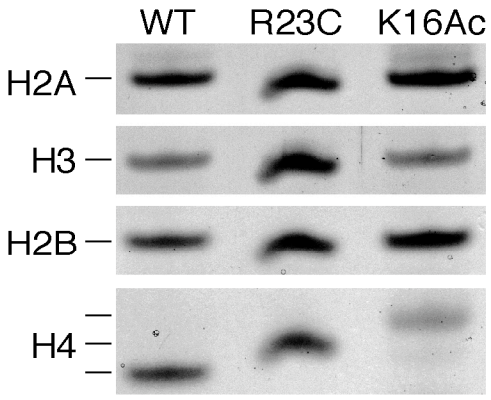

Supplemental Figure 2

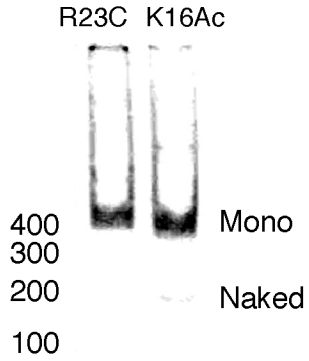

Supplemental Figure 3